Capillary bridging and long-range attractive forces in a mean-field approach

D. Andrienko,[1] P. Patrício,[2,3] and O. I. Vinogradova[1,4]

[1]*Max-Planck-Institut für Polymerforschung, Ackermannweg 10, D-55128 Mainz, Germany*
[2]*Centro de Física Teórica e Computacional, Universidade de Lisboa,*
Avenida Professor Gama Pinto 2, P-1649-003 Lisboa Codex, Portugal
[3]*Instituto Superior de Engenharia de Lisboa, Rua Conselheiro Emídio Navarro 1, P-1949-014 Lisboa, Portugal*
[4]*Laboratory of Physical Chemistry of Modified Surfaces, Institute of Physical Chemistry,*
Russian Academy of Sciences, 31 Leninsky Prospect, 119991 Moscow, Russia
(Dated: February 2, 2008)

When a mixture is confined, one of the phases can condense out. This condensate, which is otherwise metastable in the bulk, is stabilized by the presence of surfaces. In a sphere-plane geometry, routinely used in atomic force microscope (AFM) and surface force apparatus (SFA), it can form a bridge connecting the surfaces. The pressure drop in the bridge gives rise to additional long-range attractive forces between them. Minimizing the free energy of a binary mixture we obtain the force-distance curves as well as the structural phase diagram of the configuration with the bridge. Numerical results predict a discontinuous transition between the states with and without the bridge and linear force-distance curves with hysteresis. We also show that similar phenomenon can be observed in a number of different systems, e.g. liquid crystals and polymer mixtures.

I. INTRODUCTION

Capillary condensation is a classical example of a well-studied phenomenon in nature [1]. It is usually observed in a porous medium with hydrophilic surfaces, where water condenses out above its bulk transition temperature. The opposite effect, that is capillary evaporation, is observed when the surfaces are hydrophobic.

First explained by Lord Kelvin for the case of vapor-water coexisting phases, capillary condensation was also observed in other two phase gas-liquid systems and studied in various confining geometries [2, 3, 4, 5]. In fact, capillary condensation exists in any confined system close to the transition point (binodal) provided that the surfaces prefer one of the phases over the other and the bulk transition is of the first order. In this situation the condensed phase is stabilized by the presence of the surfaces in the region of the phase diagram where the condensed *bulk* state is metastable.

Interest in capillary condensation phenomenon has recently been renewed due to the fast development of high-precision force measuring devices, such as atomic force microscope (AFM) and surface force apparatus (SFA). Indeed, accurate measurements of the interactions between surfaces separated by thin fluid films led to a discovery of unexpectedly strong and long-range attraction in some systems. In many cases, direct or indirect measurements proved that these attractive interactions are due to the formation of a capillary bridge. Below we mention some examples where, in our opinion, bridging could play an important role:

(i) *attraction between hydrophobic surfaces:* Early SFA measurements revealed the presence of an attractive interaction between hydrophobic surfaces in aqueous solutions [6, 7, 8, 9]. These conclusions were confirmed by later AFM experiments [10, 11, 12, 13]. This attraction is much larger than could be expected for a van der Waals force. As a typical example, the observed range

of force for silanated surfaces was up to 400nm with the maximum attraction or adhesion (normalized by radius of interacting surfaces) about 250mN/m [11]. It has soon became clear that conventional theories of colloidal interactions fail to explain such a long-range effect [14, 15, 16].

Alternatively, it has been suggested that in some systems the hydrophobic attraction is associated with the nucleation of dissolved gas (gas-filled nanobubbles or drying film) at the surfaces [17]. When the surfaces become close, these form a gaseous bridge between them [18, 19, 20], which generates the attractive capillary force. This scenario was confirmed indirectly, from the presence of the discontinuous steps in the force curves, variability in the jump separations, hysteresis between approach and retraction, and sensitivity to dissolved gas or another solute [11, 12, 21], as well as from more direct experiments [22, 23, 24, 25, 26].

Contrary to the conclusions made on the basis of experimental data, no consensus was achieved in the theoretical description of capillary interactions. Although on purely thermodynamic ground cavitation is expected to occur between hydrophobic surfaces, both early theory [27] and later Monte Carlo study [28] predict that this should happen only when the separation becomes very small (i.e. comparable to the range of van der Waals force). The long-range capillary force was predicted only for a situation, where pre-existing hemispherical bubbles (of height and radius comparable to the range of expected attraction) are postulated on an isolated surface [29]. Contrary to this, it has been shown that the pre-formed nanobubbles are unstable and tend to dissolve very fast [30, 31, 32]. This led to speculations that the hydrophobic attraction is essentially a non-equilibrium force [13].

(ii) *nematic liquid crystals:* An exotic, but rather important example of capillary bridging has recently been observed in nematic liquid crystals [33, 34, 35]. Here the two phases forming the bridge are both liquids with

approximately the same density; the main difference between them is a degree of *orientational* molecular ordering: anisotropic molecules are orientationally *disordered* in an isotropic phase; in a nematic phase they are oriented along some preferred orientation, called the director. The fact that the two phases have different symmetry implies that the nematic-isotropic transition is of the first-order [36]. It was confirmed [37] that, in the frame of the Landau-de Gennes mean-field approach, the bridge of the nematic phase is formed between two spherical particles immersed in an isotropic phase, once the system is close to the nematic-isotropic transition.

(iii) *various mixtures:* More complex in composition, strongly confined fluids, when brought close to the phase separation, often have similar features in the force-distance profiles: the force has an unprecedentedly long-range attraction with a clear hysteresis on retraction/approach. For instance, capillary bridging was observed in bicontinuous microemulsions [38] and in a solution of polymer mixtures [39].

The importance of capillary bridging as a possible driving force in colloidal systems [4, 5, 40, 41] cannot be overestimated. The formation of the condensate between the particles can trigger their aggregation and, as a result, flocculation in colloidal suspensions. Small amount of added fluid generates, through capillary effect, strong adhesive forces between the grains of granular materials [42, 43, 44].

The direct optical measurements of the bridge parameters are impossible, due to its submicroscopic size. One can study only the indirect consequences, e.g. force-distance curves in AFM or SFA experiments, and from there attempt to deduce some of the system properties. This requires theoretical modeling that fills in the gap.

The aim of this paper is to study the general consequences of the formation/annihilation of a capillary bridge upon change of the thermodynamical parameters or geometry of the system. Considering that recent experimental results on capillary condensation/evaporation are performed using AFM or SFA setups, we work in a sphere-plane geometry which is relevant for the above-mentioned techniques. We first treat the problem in a sharp-interface limit and derive simple analytical expressions for the structural phase diagram and forces in Sec. II. Then, in Sec. III, we use the Landau mean-field approach and solve the full nonlinear equations for the bridge shape numerically. In the final Section V, using simple mapping of the free energies, we discuss implication of our results to nematic liquid crystals.

II. SHARP INTERFACE LIMIT

To begin with, we construct a crude analytical solution that will give us some qualitative picture of what is happening with the bridge when the geometry or thermodynamical parameters of the system change. The approach we shall follow was proposed by Petrov et. al. [38].
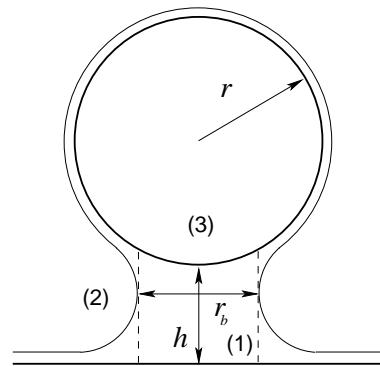

FIG. 1: Illustration of the studied geometry and bridge parametrization. Condensate of the phase (1) is stabilized between the apex of the sphere and the flat substrate. Axial symmetry is assumed throughout the paper.

To keep the description as simple as possible, we neglect the internal structure of the interfaces. Then our system involves domains of well-defined phases separated by infinitely thin interfaces, so called "sharp-interface limit" [45].

A geometry typical for SFA and AFM measurements is depicted in Fig 1. At the moment of capillary condensation the condensed phase is formed between the apex of the sphere and the flat substrate. For convenience, we denote the phase inside the bridge as a phase (1) and the bulk phase as a phase (2). We also assume that the sphere and the plane are made of the same material and denote it as a phase (3). Then the excess free energy, i.e. the change in the free energy of the system due to the emergence of the phase (1) (bridge) out of the bulk phase can be written as the sum of the bulk and surface terms

$$\Delta G = G_b + G_s. \tag{1}$$

In the sharp-interface limit, the surface free energy G_s is due to different surface tensions of the interfaces between the phases 1/3 and 2/3, plus the energy of the interface between the phases (1) and (2), which is proportional to the perimeter of the bridge

$$G_s = S_1(\sigma_{1,3} - \sigma_{2,3}) + S_2\sigma_{1,2}, \tag{2}$$

where S_1 and S_2 are the areas of the interfaces between the phases 1/3 and 1/2 correspondingly.

Additionally, we assume that the phase (1) wets the surfaces, i.e. the sphere and the plane are covered by thin wetting layers of the phase (1). This implies that the phase (1) has zero contact angle and therefore, according to the Young equation

$$\sigma_{1,3} - \sigma_{2,3} = -\sigma_{1,2}. \tag{3}$$

Note that here we implicitly assumed that we are below the prewetting transition line, i.e. the layers of the

metastable phase are thin and we can neglect their contribution to the total free energy.

The bulk free energy is due to the difference in the chemical potentials of the phase-separated component inside the bridge and in the bulk

$$G_b = V\Delta\mu, \tag{4}$$

where V is the volume of the bridge.

To calculate the surface areas and the volume of the bridge, its circumference is approximated to a cylinder, instead of the correct, concave shape. Similar approximation was used before [29]. In fact, for the typical dimensions of the surfaces and separations of SFA experiments this approximation works very well [38]. The surface areas and the volume of the bridge then read

$$
\begin{aligned}
S_1 &= 2\pi r l + \pi r_b^2, \\
S_2 &= 2\pi r_b(l + h), \\
V &= \pi r_b^2(l + h) - \frac{\pi}{6}l(3r_b^2 + l^2),
\end{aligned}
\tag{5}
$$

where $l = r - \sqrt{r^2 - r_b^2}$.

It is convenient to introduce a new constant with dimension of length

$$\lambda = \sigma_{1,2}/\Delta\mu, \tag{6}$$

and scale out the variables with dimension of length by defining

$$
\begin{aligned}
\tilde{r} &= r/\lambda, \\
\tilde{r}_b &= r_b/\lambda, \\
\tilde{h} &= h/\lambda,
\end{aligned}
\tag{7}
$$

We also introduce a dimensionless radial extent of the bridge which plays a role of the order parameter in our system

$$x = r_b/r \in [0..1]. \tag{8}$$

With this notations, the excess free energy (1) can be written as

$$\Delta G(r, r_b, h, \lambda) = \Delta\mu\lambda^3 G(x, \tilde{r}, \tilde{h}). \tag{9}$$

For every fixed $\tilde{r}, \tilde{h}$, the minimum of $G(x, \tilde{r}, \tilde{h})$ gives the equilibrium radius of the bridge.

In what follows it will be understood that scaling (7) has been carried out, and we shall omit the tildes in the text below.

Now that the mathematical problem is formulated, we first analyze the dependence of the excess free energy on the bridge radius r_b, which is shown in Fig. 2. It is similar to the Landau free energy as it occurs for phase transitions with a scalar order parameter x. It predicts a discontinuous transition between the bridged ($x > 0$) and unbridged ($x = 0$) configurations on approach/retraction of the sphere from the plane. The first-order character
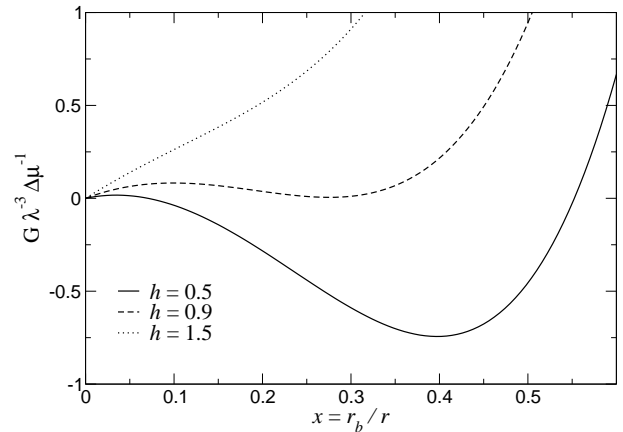

FIG. 2: Typical dependence of the excess free energy $G(x, r)$ on the radial extent of the bridge for $r/\lambda = 10$. Three separations are shown: $h = 0.5\lambda$, when the bridge is stable; $h = 0.9\lambda$, with metastable bridge; $h = 1.5\lambda$, when the configuration with the bridge is unstable.

of the transition indicates possible jumps and hysteresis in force-distance curves measured in AFM and SFA experiments [11, 12, 18, 19, 20].

Let us now localize the transition line. The equilibrium radius of the bridge corresponds to the minimum of the excess free energy $G(x, r, h)$. In addition, the configuration with the bridge is energetically preferable if $G(x_t, r, h_t) < 0$. Therefore, the following equations determine the transition line (binodal in a thermodynamical sense)

$$\frac{\partial G}{\partial x}(x_t, r, h_t) = 0, G(x_t, r, h_t) = 0. \tag{10}$$

The configuration with the bridge (or without it) can also be *metastable*, when it is a *local* minimum of the excess free energy. The corresponding metastability limits (spinodals) can be determined from the condition

$$\frac{\partial G}{\partial x}(x_m, r, h_m) = 0, \frac{\partial^2 G}{\partial x^2}(x_m, r, h_m) = 0. \tag{11}$$

Now that we have a criteria for the stability and the metastability of the bridge, Eqns. (10,11), let us have a look at the dependence of the bridge radius r_b/r on the sphere-plane separation, h. If we differentiate the excess free energy $G(x, r, h)$ with respect to x, we find that the extrema of the free energy are solutions of the implicit equation for the bridge radius

$$h = r\left(\sqrt{1 - x^2} - 1\right) + \frac{x}{r^{-1} + x}\left(\sqrt{\frac{1 - x}{1 + x}} + 1\right). \tag{12}$$

These solutions are shown in Fig. 3 for several values of the sphere radius r. As anticipated, there are two solutions for each separation $h < h_m(r)$, which correspond to two extrema of the excess free energy (see Fig. 2). The
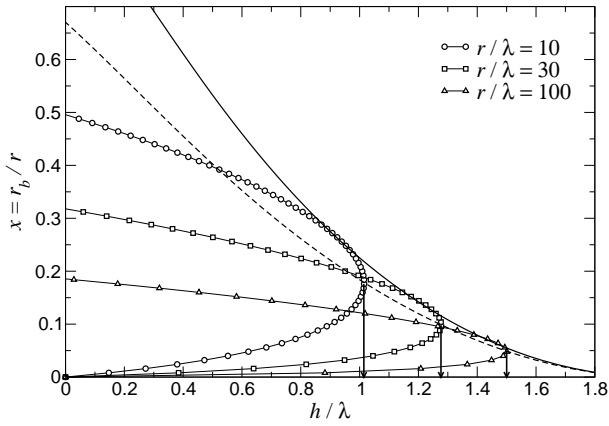
FIG. 3: Bridge radius r_b/r as a function of the sphere-plane separation h/λ. The curves correspond to the different radii of the sphere $r/\lambda = \{10, 30, 100\}$. Solid and dashed lines are binodal and spinodal correspondingly.

FIG. 4: Structural phase diagram of the capillary bridge. For small r/λ the bridge becomes unstable already for small separations h/λ. For large r/λ the threshold separation asymptotically approaches 2λ. Solid (dashed) line shows binodal (spinodal) correspondingly. Symbols presents the results of the numerical minimization. Note log scale for the sphere radius r.

larger of these two values corresponds to the minimum of the free energy; its value defines the radius of the stable (or metastable) bridge. If the separation h is larger than some value, $h_m(r)$, then the solution to Eq. (12) does not exist. Separation $h_m(r)$ provides, therefore, metastability limit for the configuration with the bridge.

Calculating the first derivative of G at $x = 0$ we find that $\partial G/\partial x(x = 0) = 2h \geq 0$, i.e. our model predicts that the configuration without the bridge can be stable or metastable and never unstable. Both the transition line, Eq. (10), and the metastability line, Eq. (11), are shown in Fig. 3.

Finally, we show the transition line (binodal) together with the metastability limit (spinodal) on the structural phase diagram, Fig. 4. It confirms that for small sphere radii the configuration with the bridge becomes unstable almost immediately, for very small sphere-plane separations. As the radius of the sphere grows, the transition occurs at much larger separations, approaching $h/\lambda = 2$ for $r \to \infty$. As a result, our model predicts that bridging is not possible for $h > 2\lambda$. The same conclusion was made in Ref. [38].

After the structural phase diagram is calculated, let us have a look at the force-distance curves. The interaction force can be calculated from the free energy

$$\frac{\mathcal{F}}{\Delta\mu\lambda^2} = -\frac{\partial G(x, r, h)}{\partial h} = -\pi r(2x + x^2 r), \quad (13)$$

and, together with equation (12), provides the force-distance curves written in parametric form.

This dependence is shown in Fig. 5, together with metastability limits and the transition line. It quantifies our previous conclusion that the transition is of the first order: for small separations the configuration with the bridge is stable and gives rise to practically linear increase of the force with separation. At the transition point this configuration becomes metastable and the bridge can dis-
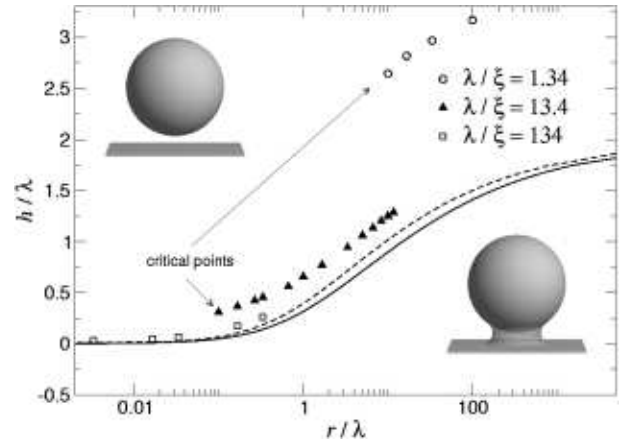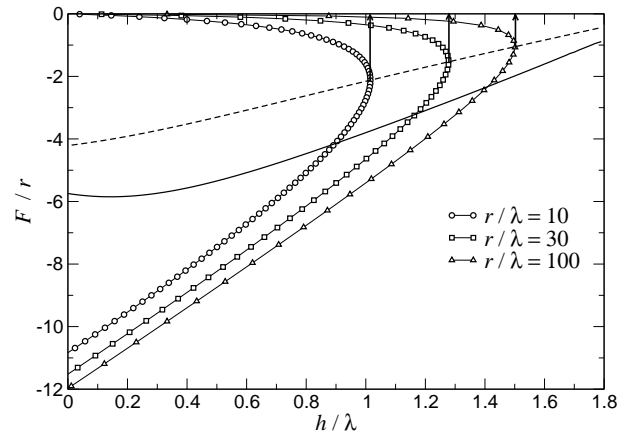

FIG. 5: Force-distance curves. Different symbols correspond to different radii of the sphere $r/\lambda = \{10, 30, 100\}$. Solid and dashed lines are binodal and spinodals correspondingly.

appear as soon as the fluctuations of the bridge radius are big enough to destroy it. Finally, at even larger separations, the bridge becomes completely unstable and disappears. There is no interaction between the sphere and the plane from this point on and the force jumps to the zero value.

On the other hand, when the sphere approaches the surface, the configuration without the bridge is stable (metastable) up to the zero separation. Therefore, the largest hysteresis in force-distance curves on approach/retraction is given by $h_m(r)$.

Before presenting the numerical results, let us briefly recall the main conclusions. Assuming that the interface is infinitely sharp and the bridge has a cylindrical shape,

we are able to see the first-order structural transition between the configurations with and without the bridge. Structural phase diagram reveals that for small sphere radii the transition occurs almost immediately, for small sphere-surface separations. On the other hand, even for large sphere radii, bridging is not possible for $h > 2\sigma/\Delta\mu$. The first-order nature of the transition leads to hysteresis in the the force-distance curves on approach/retraction of the sphere from the surface. The attractive force is basically proportional to the separation, with small deviations close to the transition line.

III. MEAN-FIELD APPROACH

It is clear that even the primitive model considered above allows a qualitatively rich description of the transition. However, there are still several important details missing, on the first place: (i) the non-cylindrical shape of the bridge; (ii) the finite thickness of the interface; (iii) the interaction between the fluid and the solid walls. Inclusion of these corrections makes the problem rather involved and does not allow anymore for a simple analytical solution. In what follows we use numerical methods to tackle the problem.

A. Free energy

To describe the bulk phase as well as the interface structure, mean-field theories [46] are often used. In this approach the order parameter ϕ is introduced. For a liquid-vapour model ϕ is just the density. For a binary mixture ϕ is a composition variable, defined as $\phi = (n_1 - n_2)/(n_1 + n_2)$, where the n_i are the number densities of the two species. This order parameter varies slowly in the bulk regions and rapidly on length scales of the interfacial width. The unmixing thermodynamics is described via a free energy functional.

In the mean-field approach the semi-grand potential of a binary mixture is written as [47]

$$\Omega\{\phi\} = \int dV \left[\frac{k}{2} \left(\nabla\phi\right)^2 + f(\phi) - \Delta\mu\phi \right], \qquad (14)$$

where $f(\phi)$ is the Helmholtz free energy density of the mixture, while $\Delta\mu$ is the chemical potential thermodynamically conjugate to the order parameter ϕ.

Since the material is confined in a container in any experiment, phase separation is always affected by surface effects [2, 3]. To include them, appropriate surface terms responsible for the interaction of the liquid with the container walls are added to the free energy [46, 47, 48]. We shall note that the surface terms are very important: they give rise to a prewetting transition and, together with $\Delta\mu$, determine the thickness of the wetting layer. However, the prewetting transition occurs only in the vicinity of the *bulk* phase separation (binodal), i.e. close

to $\Delta\mu = 0$, while capillary bridging can be observed in the whole region of the phase diagram between the spinodal and the binodal. To avoid additional complications related to the wetting/prewetting transitions, we assume that our system is below the prewetting transition line (i.e. we have thin wetting films) and fix the surface value of the order parameter to its bulk value in the infinite system.

The explicit form of the Helmholtz free energy $f(\phi)$ varies depending on the type of mixture. However, the simple observation that the two phases must coexist implies that there are two minima in the free energy at the respective values of the order parameter. Here we adopt the mean-field model for a symmetric mixture [49, 50]

$$f(\phi) = -\frac{a}{2}\phi^2 + \frac{b}{4}\phi^4. \qquad (15)$$

Note that this is one of the simplest models to describe unmixing; a more realistic description would need a more sophisticated function, which also takes into account a dependence on the overall density.

The term $(\nabla\phi)^2$ is needed to provide spatial structure to the theory: at phase coexistence, there are two bulk equilibrium order parameter values ϕ_+ and ϕ_- with the same free energy density, $f(\phi_+) = f(\phi_-)$. Without the gradient term, a structure with a large number of interfaces between the ϕ_+ and ϕ_- phase would be entropically favored. The term $(k/2)\left(\nabla\phi\right)^2$ is the simplest one which penalizes interfaces. While this is justified near the critical point, where interfaces are very wide and the order parameter varies smoothly, a more realistic description at strong segregation (where the interface becomes rather sharp) would require higher–order gradients, too.

For the free energy (15) the binodal is given by $\Delta\mu = 0$. Two spinodals (metastability limits) are located at $\Delta\mu = \pm 2a^{3/2}/(27b)^{1/2}$.

Finally, we should take into account the interaction between the solid walls and the fluid. To simplify our model, we have chosen an interaction that acts locally at the solid-fluid interface, imposing fixed boundary conditions at the walls, $\phi = \phi_-$.

B. Minimization procedure

The phase-field models are very convenient because no explicit boundary tracking is needed. However, they are wasteful in terms of simulating bulk regions. One can remedy the situation by taking into account that the order parameter varies slowly in bulk regions and rapidly on length scales of the order of the correlation length, near the interfaces. In this situation, finite elements method with adaptive mesh size solves the problem of computational efficiency: fine meshing is used only in the interfacial regions; bulk regions are coarse-grained and have much larger size of finite elements.

The equilibrium distribution of the order parameter ϕ is obtained by minimizing the free energy functional (14)

numerically using finite elements with adaptive meshes. During the minimization the square integration region $L \times L$ was triangulated using the BL2D subroutine [51]. The function ϕ is set at all vertices of the mesh and is linearly interpolated within each triangle. The free energy is then minimized using the conjugate gradients method [52] under the constraints imposed by the boundary conditions.

A new adapted mesh is generated iteratively from the previous minimization. The new local triangle sizes are calculated from the variations of the free energy, in order to guarantee a constant numerical weight for each minimization variable [53]. The final meshes, with a minimal length of $\sim 10^{-3}$, had around 10^4 minimization variables.

In order to obtain both stable and metastable configurations, we used different types of initial conditions including configurations with the capillary bridge and without it. To select stable solutions, we calculated the grand potential of the mixture, Ω, for both stable and metastable solutions and chose the solution with the lowest grand potential. This allows the accurate determination of the phase diagram.

IV. NUMERICAL RESULTS

A. Free interface

To test the minimization algorithm and to tune the minimal mesh size we first consider a system without a spherical particle and a surface. We impose the boundary conditions in such a way that a flat interface sets in the system, located at $z = 0$, perpendicular to the z axis.

In this geometry the order parameter ϕ depends only on the z coordinate and the interface profile is a solution to the following Euler-Lagrange equation

$$-k\frac{\partial^2 \phi}{\partial z^2} + \frac{\partial f}{\partial \phi} = 0, \quad (16)$$

together with the boundary conditions $\phi(\pm\infty) = \pm\phi_b$, where $\pm\phi_b$ are the homogeneous bulk solutions, given by $\partial f/\partial \phi = 0$

$$\phi_\pm = \pm\phi_b = \pm\sqrt{a/b}. \quad (17)$$

The solution to the boundary problem (16) yields

$$\phi = \phi_b \tanh(z/\xi), \quad (18)$$

where $\xi = \sqrt{2k/a}$ is the correlation length, which serves as a measure of the thickness of the interface.

With the solution (18) we go back into the free energy (14), integrate over the z coordinate and obtain the interfacial tension σ, defined as the excess free energy of the interface

$$\sigma = k\int_{-\infty}^{\infty}\left(\frac{\partial \phi}{\partial z}\right)^2 dz = \frac{2}{3}a\phi_b^2\xi. \quad (19)$$
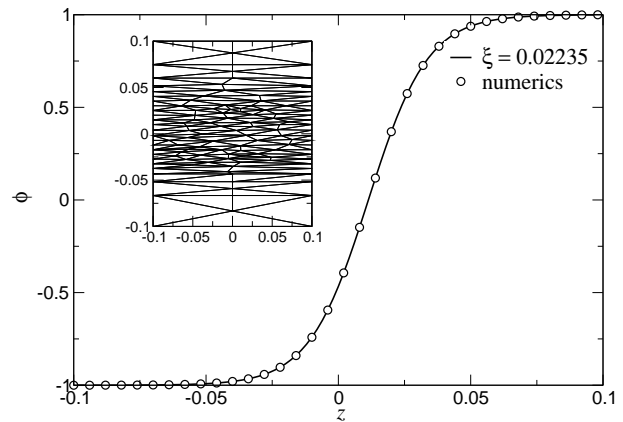

FIG. 6: Order parameter profile of a free interface. Circles: results of the numerical minimization; solid line: fit to Eq. (18) with $\xi = 0.02235$. Inset illustrates the adaptive mesh: smaller triangles are used in the interface region with strong variation of the order parameter.

For our numerical minimization we used the following parameters of the potential (14): $a = b = 4$, $k = 0.001$. They yield the correlation length $\xi \approx 0.02236$ and the interfacial tension $\sigma \approx 0.06$.

The order parameter profile for this set of parameters is shown in Fig. 6. As expected, the order parameter changes between two bulk values $\pm\phi_b = \pm 1$ and the width of the interface is of the order of the correlation length ξ. A fit of the results of the numerical minimization to Eq. (18) yields $\xi = 0.02235$, practically indistinguishable from the exact value $\sqrt{2k/a}$.

The interface thickness ξ sets the smallest length-scale in our system and, therefore, defines the minimal size of the mesh. We found that a minimal length of the final meshes $\ell = 10^{-3}$, which is about 20 mesh points per interface, is accurate enough to recover the interface structure.

The correlation length ξ and the interfacial tension σ are two parameters of our system which can be experimentally measured. In addition, the interfacial tension enters the sharp-interface description presented above. It is, therefore, convenient to rewrite the excess free energy in terms of these two parameters. This shall help us to compare the numerical results to the sharp-interface limit as well as to the existing experiments.

Performing the substitution $\psi = \phi/\phi_b$ we obtain the semi-grand potential density in the form

$$\omega = \frac{3}{8}\frac{\sigma}{\xi}\left[\xi^2\left(\frac{\partial \psi}{\partial z}\right)^2 - 2\psi^2 + \psi^4 - \frac{4}{3}\frac{\xi}{\lambda}\psi\right]. \quad (20)$$

As before, we introduced a constant

$$\lambda = \frac{\sigma}{2\Delta\mu\phi_b} \quad (21)$$

with dimension of length. Note that the length λ has (approximately) the same value as in the sharp-interface

limit. To prove this, consider the situation when $\xi \to 0$. Then the interface is sharp and the part of the excess free energy which scales as the bridge volume can be written as

$$f_{ex} = [\Delta\mu(\phi_+ - \phi_-) + f(\phi_-) - f(\phi_+)]V, \qquad (22)$$

where V is the volume of the bridge. For small chemical potential differences $\phi_\pm \approx \pm\phi_b$, where ϕ_b is the value of the order parameter when $\Delta\mu = 0$. Then f_{ex} can be rewritten as $2\Delta\mu\phi_b V$. Comparing f_{ex} to the expression for the bulk free energy in the sharp interface limit, Eq. (4), we obtain the definition of λ in the form of Eq. (21).

Now that the semi-grand potential density is written in a dimensionless form it is clear that there is an additional length-scale in the problem, when it is formulated in the phase-field approach. This length-scale is the correlation length ξ or, alternatively, the width of the interface between the two phases.

Three more variables with dimension of length are present in the problem. Two of them, sphere radius r and sphere-plane separation h, fix the geometry of the system. For both SFA and AFM experiments $r \gg h$. The third variable, λ, specifies the thermodynamic state of the system. The thickness of the interface ξ validates the sharp-interface limit: it is applicable only when $\xi \ll \lambda, h, r$.

B. Sphere-plane geometry

We have thus seen that the interface thickness ξ sets the length-scale in our system. Therefore, three dimensionless ratios uniquely specify the state of the system: r/ξ, h/ξ, and λ/ξ. In what follows we fix the thickness of the interface to $\xi = 0.02235$; the corresponding constants of the potential are discussed in Section IV A. The rest of the parameters with dimension of length (i.e. r, h, λ) are given in units of ξ.

Let us first look at the situation when the thermodynamic parameters of the system (i.e. λ, in addition to ξ) are fixed, but the geometry is changing. For these calculations we used the chemical potential difference $\Delta\mu = 0.1$, which yields $\lambda/\xi \approx 13.4$.

The functional (14) was minimized for a range of sphere radii, $r/\xi \in [0.5..200]$ with the boundary conditions $\phi = \phi_-$ at the sphere and the plane surfaces. Note that the smallest size of the sphere is naturally set by the phenomenological description we use: it is not applicable on length-scales much smaller than the interface width ξ. The upper value is limited by the computational capacities: further increase in the sphere radius led to significant slowdown of already rather time-consuming calculations.

Typical cross-sections of the bridge are shown in Fig. 7. For small sphere-plane separations the wetting film, covering the sphere and the plane, becomes thicker next to the sphere, Fig. 7(a). On retraction of the sphere from
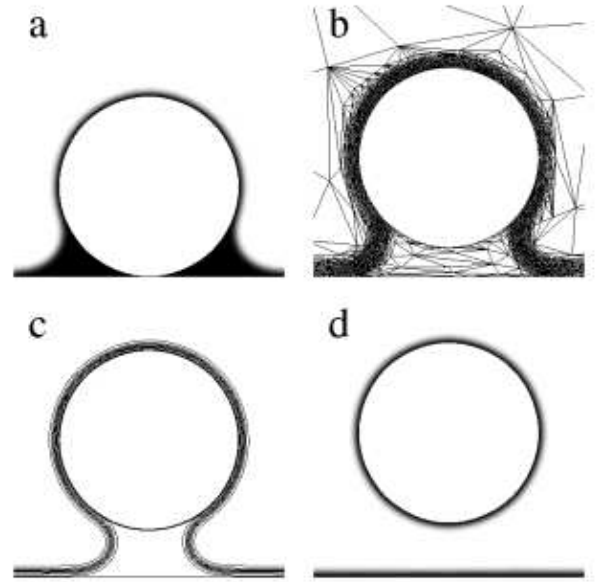

FIG. 7: Cross-section of a capillary bridge for several surface-tip separations: $h/\xi = \{0, 7.16, 11.63, 13.42\}$. Sphere radius $r/\xi = 22.36$, $\lambda/\xi = 13.42$. b) illustrates the final mesh; c) shows the interface contour lines, which are parallel to the surface of the bridge.

the plane the bridge is formed and then gradually thinners, see Figs. 7(b) and (c). Finally, at even larger separations, the bridge becomes unstable and disappears. The configuration with the sphere and the plane, wetted by a thin wetting layer, Fig. 7(d), becomes energetically favorable. At these distances the sphere and the plane no longer interact with each other.

To investigate the nature of the structural transitions between the bridged and unbridged configurations, we plot the excess free energy as a function of the sphere-plane separation h in Fig. 8.

The free energy profiles quantify the conclusions made above: when the sphere is far from the plane, the configuration without the bridge is the only stable one. The excess free energy does not change with separation, i.e. there is no force acting on the sphere. When the sphere moves closer to the plane, this configuration becomes first metastable, and then unstable. The bridge is formed and stays until the sphere touches the surface.

On the other hand, on retraction, the configuration with the bridge becomes first metastable and then unstable. Jump in the free energy profile points on discontinuous (first-order) structural transition between the configurations with and without the bridge. Due to the first-order nature of the transition, the configuration with the bridge can be kinetically stabilized and the bridge can, in principle, disappear at any position where it is metastable. In fact, this explains the variability in the jump-in/out distances observed in experiment [11, 18, 20].
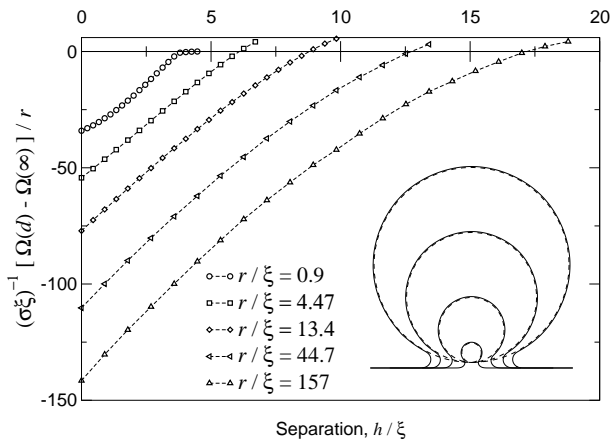
FIG. 8: Excess free energy of the configuration with the bridge vs sphere-plane separation. Different curves correspond to different sphere radii. Inset illustrates change in the radial extent and shape of the bridge when the sphere radius changes. The inset configurations are taken at a fixed sphere-surface separation, $h/\xi = 8.94$.

FIG. 9: Force-distance curves calculated for several dimensionless sphere radii r/ξ. Inset shows the slope of the curves α vs the sphere radius r.

On the face of it, the scenario predicted by the phase-field approach is similar to the previous, sharp-interface limit one. However, in addition to quantitative corrections, it also predicts *qualitatively* different results for small r/ξ. Indeed, as it is seen from the free energy profile for $r/\xi = 0.9$, there is no jump in the excess free energy. Instead, we have a smooth cross-over between the bridged configuration and configuration without the bridge. This points to a critical point r_c below which the bridge will no longer disappear discontinuously. The difference between the phase-field and the sharp-interface approaches for $r/\xi \approx 1$ is, of course, expected, since the infinitely sharp interface assumption breaks down when the radius of the sphere is of the order of the correlation length ξ. It is then tempting to explain the absence of a jump in computer simulations [28], where the system sizes are typically limited to thousands of angstroms.

To calculate the transition line, we fitted the free energy profiles with a simple polynomial dependence (quadratic polynomial turned out to be a reasonable approximation) and found where it intersects the $\Omega = 0$ axis. This allows accurate determination of the transition line. The results are shown in Fig. 4, together with the structural phase diagram obtained in the sharp-interface limit. The agreement above the critical point is reasonable, taking into account that we made rather crude approximations about the shape of the bridge in the sharp interface limit.

We have thus seen that the excess free energy profiles, scaled out by the sphere radius, are accurately fitted by a quadratic polynomial. For large r/ξ these profiles have *convex* shape pointing that the attractive force, which is the first derivative of the excess free energy with respect to the sphere-plane separation, *decreases linearly* with the increase of the sphere-plane separation. It can be also
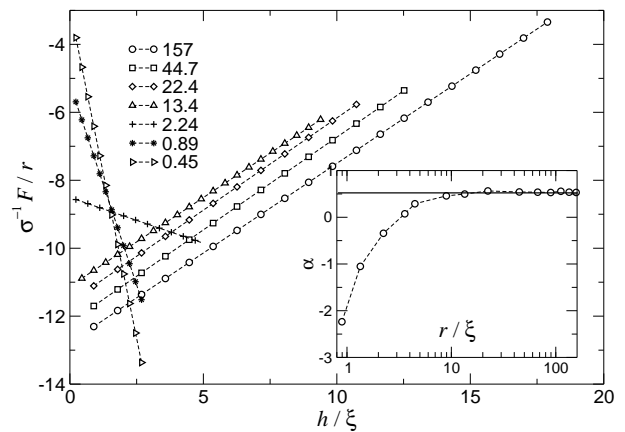
seen that the free energy profiles, when scaled out by r, are almost parallel to each other, especially for $r/\xi \to \infty$. This means that the *slope* of the force, scaled by the sphere radius r, approaches asymptotically a constant value when $r/\xi \to \infty$. For smaller r/ξ the force profiles become first *linear* in h and then start to curve inwards, changing their shape to *concave*. As a result, the force is independent of h for some particular sphere radius; for even smaller r/ξ it *increases* with the increase of h.

This is illustrated in Fig. 9, where we show the force-distance curves calculated for $\lambda/\xi = 13.4$. The inset shows the slope α obtained from the linear fit

$$\mathcal{F} = \mathcal{F}_0 + \sigma\xi\alpha rh. \qquad (23)$$

Note that here both r and h are dimensionless, i. e. given in units of ξ. The fit confirms that for $r/\xi > 10$ we have a constant slope $\alpha \approx 0.5$, i.e. the force simply scales with the sphere radius r, like in the Derjaguin approximation [54].

We studied two more situations, with $\lambda/\xi = 134 \gg 1$ and $\lambda/\xi = 1.34 \sim 1$. The transition lines for both cases are also shown on the structural phase diagram, Fig. 4. For $\lambda/\xi = 134$ the agreement with the sharp interface limit is remarkably better. At the same time, it is clearly worse for $\lambda/\xi \sim 1$: the transition line is shifted toward bigger separations and ends in a critical point for rather large r/λ. There are two reasons for this. First, the shape of the bridge is, in fact, a surface of revolution whose mean curvature is constant. These surfaces are known as Delaunay surfaces, or onduloids [55]. λ defines the "radius of curvature" of the bridge cross-section through its symmetry axis. If $\lambda \gg r$ the bridge is well approximated by a cylinder. This explains good agreement with the sharp interface limit for $\lambda/\xi = 134$. On the other hand, when $\lambda \sim \xi$ the radius of curvature is of the order of the interface thickness, i.e. the sharp interface limit cannot be used, even if $r, h \gg \xi$.

In spite of the complications in the structural phase diagram for $\lambda \sim \xi$ and $r \sim \xi$, the main conclusions of our numerical studies remain: the transition between bridged and unbridged configurations is of the first order; the transition line ends in a critical point located at $r_c/\xi \sim 1$. For large spheres, $r/\xi > 10$, the force is a linear function of the sphere-plane separation h with a slope proportional to the sphere radius r.

V. EXAMPLES AND DISCUSSION

In the previous sections a theoretical and numerical analysis of the bridge formation and stability has been developed for a simple binary mixture. Here we discuss implication of our results for several different systems.

We begin with nematic liquid crystals, mentioned in Introduction. From the phenomenological point of view, the system is described by the Landau-de Gennes free energy [56]

$$F\{\boldsymbol{Q}\} = \int (f_b + f_e)dV + \int f_s dS \qquad (24)$$

where f_b is the bulk free energy density, f_e is the elastic free energy density and f_s is the surface free energy. Within a mesoscopic approach the minimum of the Landau-de Gennes functional $F\{\boldsymbol{Q}\}$ gives the equilibrium value of the tensor order parameter $\boldsymbol{Q}$.

Symmetry arguments yield for the local bulk free energy density [56, 57]

$$f_b = a\mathrm{Tr}\boldsymbol{Q}^2 - b\mathrm{Tr}\boldsymbol{Q}^3 + c\left[\mathrm{Tr}\boldsymbol{Q}^2\right]^2, \qquad (25)$$

where a is assumed to depend linearly on the temperature, while the positive constants b, c are taken temperature independent.

It is convenient to scale out the variables by defining

$$\tilde{Q}_{ij} = 6c/bQ_{ij}, \qquad (26)$$
$$\tilde{f}_b = 24^2c^3/b^4 f_b.$$

It will be understood that such scaling has been carried out, and we shall omit the overbars in the text below.

We also introduce a dimensionless temperature τ by defining

$$a = \tau b^2/24c. \qquad (27)$$

The elastic free energy density can be written as [57]

$$f_e = \frac{1}{2}L_1\frac{\partial Q_{ij}}{\partial x_k}\frac{\partial Q_{ij}}{\partial x_k} + \frac{1}{2}L_2\frac{\partial Q_{ij}}{\partial x_j}\frac{\partial Q_{ik}}{\partial x_k}, \qquad (28)$$

where the constants L_1 and L_2 are related to Frank-Oseen elastic constants by $K_{11} = K_{33} = 9Q_b^2(L_1 + L_2/2)/2$ and $K_{22} = 9Q_b^2L_1/2$ and Q_b is the bulk nematic order parameter. The sign of L_2 defines the preferred orientation of the director at the NI interface. $L_2 > 0$ ($L_2 < 0$) favors planar (perpendicular) anchoring [58].

Now that the full free energy is specified, we perform several simplifications. To begin with we neglect the non-uniformity of the director distribution inside the bridge. This assumption is quite reasonable for the studied geometry: we assume homeotropic (perpendicular) anchoring of the director at the surfaces and planar (parallel) anchoring at the nematic-isotropic interface. Second, we assume that the nematic phase is uniaxial and neglect the biaxiality of the interface. The full problem has been considered recently by Stark et. al. [37].

For a *uniform uniaxial* nematic ($Q_{11} = Q$, $Q_{22} = Q_{33} = -1/2Q$) the free energy (25) takes the form

$$f_b = \tau Q^2 - 2Q^3 + Q^4. \qquad (29)$$

Free energy (29) predicts that the nematic state is stable when $\tau < \tau_{\mathrm{NI}} = 1$ with a degree of orientational order given by

$$Q_b = \frac{3}{4}\left(1 + \sqrt{1 - \frac{8}{9}\tau}\right), \qquad (30)$$

The same expression provides us with the metastability limit of the nematic phase on heating at $\tau^* = 9/8$.

The solution which corresponds to a free interface is then given by the de Gennes Ansatz [58],

$$Q = \frac{1}{2}\left(1 + \tanh\frac{z}{\xi}\right), \qquad (31)$$

where ξ is the nematic correlation length when the director is parallel to the interface

$$\xi^2 = \frac{8L_1c}{b^2}\left(6 + \frac{L_2}{L_1}\right). \qquad (32)$$

A linear transformation of the order parameter, $Q = (1 + \phi)/2$, reduces the Ansatz (31) to the familiar form (18). The same substitution transforms the free energy of a uniaxial nematic to the free energy of a binary mixture

$$f_b = [\phi^4 - 2(3 - 2\tau)\phi^2 + 8(\tau - 1)\phi]/16. \qquad (33)$$

Close to the nematic-isotropic transition, $\tau_{\mathrm{NI}} = 1$, the τ-dependence of the coefficient at ϕ^2 is not important, and the free energy has exactly the same form as (21) provided that

$$\lambda = \frac{\xi}{6(\tau - 1)}. \qquad (34)$$

This is an interesting result: recalling that the nematic-isotropic transition occurs at $\tau_{\mathrm{NI}} = 1$ and the superheating temperature of the nematic phase $\tau^* = 9/8$ we see that $\lambda \geq 4/3\xi$, i.e. λ spans the whole range of values, from the interface thickness ξ at the superheating temperature, to the system sizes, set by the sphere radius r and the sphere-plane separation h, and diverges at the

nematic-isotropic transition. This implies that, depending on the temperature, one can have either discontinuous (first-order) or continuous transition between bridged and unbridged configurations. Moreover, by changing the temperature of the liquid crystal it is possible to control the range and the strength of the attractive force between the particles in colloidal suspensions.

Another 'liquid crystalline' example for which our results are relevant is drag of colloidal particles by the nematic-isotropic interface. Recent experiments [59] revealed that the nematic-isotropic interface is able to drag colloidal particles and, as a result, form spatial patterns in the liquid crystal cell. Theoretical reexamination of the experimental data [60] demonstrated that the force exerted on a colloidal particle is proportional to the penetration depth, and the slope of the force scales as the particle size r. This points to rather unexpected mapping: here the bridge connects the colloidal particle and the interface itself, since the position of the latter is fixed by a small temperature gradient present in the system. The straightforward implication of our results, which is also confirmed experimentally [59], is that it is more difficult for the interface to capture small particles. Indeed, the attractive force from the side of the interface scales with radius. In addition, the barrier becomes smaller, completely vanishing at the critical radius r_c.

Finally, we would like to mention that the standard Flory-Huggins expression for a free energy of an incompressible polymer mixture [61, 62] can be expanded in powers of the polymer volume fraction ϕ. Close to the critical point it has the same form as (15) with $a = -k_B T/N + \chi/2, b = k_B T/(3N)$, where χ is the Flory-Huggins parameter, N is the effective chain length. This means that the whole picture of bridging, described here, can be adapted for the case of incompressible polymer mixtures. In fact, the capillary-induced phase separation in binary polymer solutions has been experimentally observed [39] and theoretically studied using mean-field lattice modeling [63].

In many ways the interface acts like a membrane un-

der tension. In our particular situation the formation of a bridge between the surface and a particle resembles the process of wrapping a colloidal particle by a membrane [64, 65]. A detailed comparison requires, however, further analysis.

As a final remark, we remind that, by using rigid boundary conditions, we will not observe possible prewetting transitions which have been studied in detail for simpler geometries [2, 46, 66]. These transitions normaly occur close to the bulk phase separation, i.e. when $\Delta\mu \approx 0$, or $\lambda \gg 1$. The corresponding part of the phase diagram $(r/\lambda, h/\lambda \ll 1)$ can, therefore, be affected by these effects. On the other hand, when $r \to \infty$, we recover the capillary condensation in a slab geometry [2]. In fact, the critical point has similar to the capillary condensation origin: it occurs when the interfacial width is comparable to the sphere-plane separation, i. e. to the width of the capillary.

VI. CONCLUSIONS

In conclusion, we have presented a detailed study of interactions between the sphere and the plane due to formation of the capillary bridge between them. We have shown that the structural transition between the configurations with and without the bridge is discontinuous and ends in a critical point for small particle radii. We have also demonstrated that the attractive force is long-ranged and is basically proportional to the sphere-plane separation and possible hysteresis on approach/separation.

[1] H. T. Davis, *Statistical mechanics of phases, interfaces, and thin films* (VCH Publishers, New York, 1996).
[2] R. Evans, U. M. B. Marconi, and P. Tarazona, J. Chem. Phys. **84**, 2376 (1986).
[3] R. Evans and U. M. B. Marconi, J. Chem. Phys. **86**, 7138 (1987).
[4] H. T. Dobbs and J. M. Yeomans, Journal Of Physics-Condensed Matter **4**, 10133 (1992).
[5] H. T. Dobbs, G. A. Darbellay, and J. M. Yeomans, Europhysics Letters **18**, 439 (1992).
[6] J. Israelachvili and R. Pashley, Nature **300**, 341 (1982).
[7] Y. I. Rabinovich and B. V. Derjaguin, Colloids And Surfaces **30**, 243 (1988).
[8] H. K. Christenson and P. M. Claesson, Science **239**, 390 (1988).
[9] J. L. Parker, P. M. Claesson, and P. Attard, Journal Of

Physical Chemistry **98**, 8468 (1994).
[10] L. Meagher and V. S. J. Craig, Langmuir **10**, 2736 (1994).
[11] N. Ishida, M. Sakamoto, M. Miyahara, and K. Higashitani, Langmuir **16**, 5681 (2000).
[12] O. I. Vinogradova, G. E. Yakubov, and H. J. Butt, Journal Of Chemical Physics **114**, 8124 (2001).
[13] P. Attard, Advances In Colloid And Interface Science **104**, 75 (2003).
[14] J. C. Eriksson, S. Ljunggren, and P. M. Claesson, Journal Of The Chemical Society-Faraday Transactions Ii **85**, 163 (1989).
[15] R. Podgornik, Journal Of Chemical Physics **91**, 5840 (1989).
[16] P. Attard, Journal Of Physical Chemistry **93**, 6441 (1989).
[17] O. I. Vinogradova, N. F. Bunkin, N. V. Churaev, O. A.

Kiseleva, A. V. Lobeyev, and B. W. Ninham, Journal Of Colloid And Interface Science **173**, 443 (1995).

[18] A. Carambassis, L. C. Jonker, P. Attard, and M. W. Rutland, Phys. Rev. Lett. **80**, 5357 (1998).

[19] R. F. Considine, R. A. Hayes, and R. G. Horn, Langmuir **15**, 1657 (1999).

[20] G. E. Yakubov, H. J. Butt, and O. I. Vinogradova, Journal Of Physical Chemistry B **104**, 3407 (2000).

[21] A. V. Nguyen, J. Nalaskowski, J. D. Miller, and H. J. Butt, International Journal of Mineral Processing **72**, 215 (2003).

[22] N. F. Bunkin, O. A. Kiseleva, A. V. Lobeyev, T. G. Movchan, B. W. Ninham, and O. I. Vinogradova, Langmuir **13**, 3024 (1997).

[23] W. Q. Gong, J. Stearnes, D. Fornasiero, R. A. Hayes, and J. Ralston, Physical Chemistry Chemical Physics **1**, 2799 (1999).

[24] J. W. G. Tyrrell and P. Attard, Phys. Rev. Lett. **8717**, 176104 (2001).

[25] N. Ishida, M. Sakamoto, M. Miyahara, and K. Higashitani, Journal Of Colloid And Interface Science **253**, 112 (2002).

[26] R. Steitz, T. Gutberlet, T. Hauss, B. Klosgen, R. Krastev, S. Schemmel, A. C. Simonsen, and G. H. Findenegg, Langmuir **19**, 2409 (2003).

[27] V. V. Yaminsky, V. S. Yushchenko, E. A. Amelina, and E. D. Shchukin, Journal Of Colloid And Interface Science **96**, 301 (1983).

[28] H. Shinto, K. Uranishi, M. Miyahara, and K. Higashitani, Journal Of Chemical Physics **116**, 9500 (2002).

[29] P. Attard, Langmuir **16**, 4455 (2000).

[30] J. C. Eriksson and S. Ljunggren, Langmuir **11**, 2325 (1995).

[31] S. Ljunggren and J. C. Eriksson, Colloids And Surfaces A-Physicochemical And Engineering Aspects **130**, 151 (1997).

[32] J. C. Eriksson and S. Ljunggren, Colloids And Surfaces A-Physicochemical And Engineering Aspects **159**, 159 (1999).

[33] K. Kocevar, A. Borstnik, I. Musevic, and S. Zumer, Physical Review Letters **86**, 5914 (2001).

[34] K. Kocevar and I. Musevic, Physical Review E **64**, 051711 (2001).

[35] K. Kocevar and I. Musevic, Chemphyschem **4**, 1049 (2003).

[36] P. M. Chaikin and T. C. Lubensky, *Principles of Condensed Matter Physics* (Cambridge University Press, Cambridge, 1995).

[37] H. Stark, J. Fukuda, and H. Yokoyama, Phys. Rev. Lett. (2004), unpublished.

[38] P. Petrov, U. Olsson, and H. Wennerstrom, Langmuir **13**, 3331 (1997).

[39] H. Wennerström, K. Thuresson, P. Linse, and E. Freyssingeas, Langmuir **14**, 5664 (1998).

[40] V. S. Yushchenko, V. V. Yaminsky, and E. D. Shchukin, Journal Of Colloid And Interface Science **96**, 307 (1983).

[41] C. Bauer, T. Bieker, and S. Dietrich, Phys. Rev. E **62**, 5324 (2000).

[42] H. M. Jaeger, S. R. Nagel, and R. P. Behringer, Reviews Of Modern Physics **68**, 1259 (1996).

[43] T. C. Halsey and A. J. Levine, Physical Review Letters **80**, 3141 (1998).

[44] M. Schulz, B. M. Schulz, and S. Herminghaus, Physical Review E **67** (2003).

[45] K. R. Elder, M. Grant, N. Provatas, and J. M. Kosterlitz, Phys. Rev. E **6402**, 021604 (2001).

[46] K. Binder, in *Phase Transitions and Critical Phenomena*, edited by C. Domb and J. Lebowitz (Academic Press, 1983), vol. 8, pp. 2–144.

[47] D. Bonn and D. Ross, Rep. Prog. Phys. **64**, 1085 (2001).

[48] J. W. Cahn, J. Chem. Phys. **66**, 3667 (1977).

[49] L. E. Reichl, *A modern course in statistical physics* (John Wiley & Sons, New York, 1998).

[50] J. S. Rowlinson, *Liquids and liquid mixtures* (Butterworth, London, 1969), 2nd ed.

[51] P. L. George and H. Borouchaki, *Delaunay triangulation and meshing : application to finite elements* (Hermes, Paris, 1998).

[52] W. H. Press, B. P. Flannery, S. A. Teukolsky, and W. T. Vetterling, *Numerical Recipes in Fortran* (Cambridge University Press, Cambridge, 1992), 2nd ed.

[53] P. Patrício, M. Tasinkevych, and M. M. Telo da Gama, Eur. Phys. J. E **7**, 117 (2002).

[54] L. R. White, Journal Of Colloid And Interface Science **95**, 286 (1983).

[55] H. Cundy and A. Rollett, *Mathematical Models* (Tarquin Pub., Stradbroke, England, 1989), 3rd ed.

[56] P. G. de Gennes and J. Prost, *The Physics of Liquid Crystals* (Clarendon Press, Oxford, 1995), second, paperback ed.

[57] M. Stephen and J. Straley, Rev. Mod. Phys. **46**, 617 (1974).

[58] P. G. de Gennes, Mol Cryst Liquid Cryst **12**, 193 (1971).

[59] J. L. West, A. Glushchenko, G. Liao, Y. Reznikov, D. Andrienko, and M. P. Allen, Phys. Rev. E **66**, 012702 (2002).

[60] D. Andrienko, M. Tasinkevych, P. Patrício, and M. M. Telo da Gama, Phys. Rev. E **69**, 021706 (2004).

[61] K. Binder, Theories And Mechanism Of Phase Transitions, Heterophase Polymerizations, Homopolymerization, Addition Polymerization **112**, 181 (1994).

[62] T. Flebbe, B. Dünweg, and K. Binder, J. Phys. II **6**, 667 (1996).

[63] M. Olsson, P. Linse, and L. Piculell, Langmuir **20**, 1611 (2004).

[64] A. Boulbitch, Europhysics Letters **59**, 910 (2002).

[65] M. Deserno and T. Bickel, Europhysics Letters **62**, 767 (2003).

[66] S. Dietrich, in *Phase Transitions and Critical Phenomena*, edited by C. Domb and J. Lebowitz (Academic Press, 1988), vol. 12, p. 1.